Research Article GU J Sci, Part A, 11(1): 164-172 (2024) 10.54287/gujsa.1420777

Gazi University
Journal of Science
PART A: ENGINEERING AND INNOVATION
http://dergipark.org.tr/gujsa

One-pot Synthesis of Graphene Oxide-MnO_2-Polyaniline Nanocomposites and Their Photothermal Properties

Zafer ÇIPLAK[1*] Furkan SOYSAL[2]

[1] *Sivas Cumhuriyet University, Faculty of Engineering, Department of Chemical Engineering, Sivas, Türkiye*
[2] *Ankara Yıldırım Beyazıt University, Faculty of Engineering and Natural Sciences, Department of Chemical Engineering, Ankara, Türkiye*

Keywords

Graphene Oxide
MnO_2
Polyaniline
Photothermal

Abstract

Graphene oxide-MnO_2-Polyaniline ternary nanocomposites were synthesized by a facile one-pot approach and characterized with UV-Visible spectroscopy, XRD and SEM. Photothermal properties of the nanocomposite dispersions were tested with an 808 nm wavelength near-infrared laser. Efficiency of the nanocomposites were calculated with time constant method and maximum efficiency was found to be 73.9 %. Additionally, cyclic heating cooling experiments proved the superb dispersion stability and photothermal performance of the nanocomposite.

Cite

Çiplak, Z., & Soysal, F. (2024). One-pot Synthesis of Graphene Oxide-MnO_2-Polyaniline Nanocomposites and Their Photothermal Properties. *GU J Sci, Part A, 11*(1), 164-172. doi:10.54287/gujsa.1420777

Author ID (ORCID Number)

0000-0003-2449-5274 Zafer ÇIPLAK
0000-0002-2558-2014 Furkan SOYSAL

Article Process

Submission Date 16.01.2024
Revision Date 20.02.2024
Accepted Date 01.03.2024
Published Date 15.03.2024

1. INTRODUCTION

Cancer is one of the biggest medical issues, taking the lives of almost 10 million people a year (Wei et al., 2019). Surgery, chemotherapy, and radiotherapy are the main methods used in the traditional clinical treatment of cancer. Surgery is insufficient to completely remove tumor cells from the body. Chemotherapy and radiotherapy damage healthy tissues along with cancer cells and their side effects limit the patient's quality of life and treatment effectiveness. These disadvantages of traditional cancer treatment methods have led scientists to investigate alternative treatment methods that are more effective in clinical treatment and have more positive effects on the patient's quality of life (Wei et al., 2019). Photothermal therapy (PTT) is based on the idea of raising the temperature of the body region where the tumor tissue is located. Combining PTT with other forms of treatment has the potential to improve the efficacy of cancer treatment while lowering adverse effects on bodily systems (Lima-Sousa et al., 2024).

Nowadays, bacterial infections caused by drug-resistant microbes are another global health problem. 700,000 people in the world lose their lives annually, due to diseases caused by multi drug resistant bacteria (MDR) (Bai et al., 2023; Xing et al., 2024). With the rapid spread of antibiotic resistance, more bacterial species are becoming resistant to commercial antibiotics. More antibiotics lose their effectiveness every year (Guan et al., 2021). The discovery rate of new antibiotics is much slower than the increase of MDR bacteria (Bai et al., 2023). In 2050, human deaths caused by MDR bacteria are predicted to be 10 million per year (Bai et al., 2023). In recent years, unlike chemical treatments, physical approaches, such as, killing bacteria with heat and irradiation have emerged as more promising alternative methods against antibiotic resistance (Guan et al., 2021). Therefore, introducing new approaches that can replace traditional drug treatment is of great importance for public health. PTT and combined therapies containing PTT have great potential in the treatment of MDR, as in the treatment of cancer (Bai et al., 2023).

*Corresponding Author, e-mail: zaferciplak@cumhuriyet.edu.tr

Using PTT agents and near-infrared (NIR) laser to generate localized heat, as a non-invasive application, provides distinct advantages, such as, low systemic toxicity and good controllability. NIR light is in the wavelength range of 650 – 950 nm and can penetrate tissues. Additionally, NIR absorption of water and hemoglobin in the tissue is weak (Soysal et al., 2022). It is of great importance to produce photothermal agents with high photothermal conversion efficiency, high photothermal stability, low toxicity and stable aqueous dispersions that can be used in cancer treatment and antimicrobial applications.

Despite its limited photothermal properties, graphene oxide (GO) is an important composite component in the production of photoagent nanocomposites with its advantages such as excellent dispersion in aqueous environment, very large surface area, and low toxicity. GO, with its strong electrostatic and π-π interactions with metal oxide salts and monomers, prevents the agglomeration of photoagents during the nanostructure production and polymerization process, allowing them to be produced in small sizes and ultra-thin form. GO also contributes to the strong interaction of composite components with each other and with its hydrophilic feature provide effective dispersion of the composite in the aqueous media (İrez & Bayraktar, 2020).

Because of oxygen vacancies in their chemical structure MnO_2 nanomaterials can act as photoagents in NIR region for PTT applications. MnO_2 nanostructures are remarkable materials for biomedical applications due to their features such as easy synthesis, low cost and biodegradability (Liu et al., 2021). When MnO_2 reacts with hydrogen peroxide, oxygen production occurs. The Mn^{2+} ions formed by this reaction react with hydrogen peroxide again and hydroxyl radicals are directly formed (Xu et al., 2022). This feature also provides photodynamic properties to MnO_2 nanostructures and reveals significant potential for photothermal-photodynamic combined treatment applications for MnO_2-containing composites. Wang et al. (2019) fabricated Ag/chitosan/MnO_2 nanosheets and investigated photothermal properties of MnO_2 nanosheets (Wang et al., 2019). Under 808 nm NIR laser at 0.5 W/cm^2 laser power density for 10 min irradiation the temperature of 0.2 mg/mL MnO_2 suspension rised to 60 ºC and MnO_2 nanosheets exhibited photothermal conversion efficiency of 30.79%. Liu et al. (2021) enzymatically produced MnO_2 nanoparticles (Liu et al., 2021). At 1.5 W/cm^2 intensity, 0.15 mg/mL MnO_2 aqueous dispersion exhibited a photothermal conversion efficiency of 44%. Despite their good photothermal features, improvement of the PTT performance of MnO_2 nanostructures is still needed. Combining of MnO_2 with conducting polymers offers great potential for PTT applications. Conductive polymers have a much higher ability to absorb NIR light compared to graphene-based materials and metal oxides such as MnO_2. Thus, they demonstrate high temperature increase and photothermal conversion efficiency at low concentrations. Moreover, conductive polymers are promising photothermal therapy agents due to their advantages such as providing long-term photothermal stability and not causing toxicity problems (Yu et al., 2020; Pham et al., 2024). Among these conductive polymers, polyaniline (PANI) is a low-cost, biocompatible and easily produced conductive polymer, and has become the focus of attention in photothermal applications in recent years because it can demonstrate high photothermal performance.

In this study, GO-MnO_2-PANI (GMP) nanocomposite was fabricated with a facile, one-pot synthesis approach (Zeplin & Neiva, 2021). Simultaneous production of MnO_2 nanostructures and PANI conjugated polymer was realized by using $KMnO_4$ as oxidizing agent to initiate aniline monomer polymerization on the surfaces of GO nanosheets in dodecyl benzene sulfonic acid (DBSA) aqueous solution. DBSA organic acid aqueous solution, in addition to providing the doping of PANI, plays the role of stabilizing agent for the preparation of water-stable dispersions of the composite. Photothermal properties of ternary GMP nanocomposite were investigated for the first time in the literature. The nanocomposite photoagents exhibited high photothermal conversion efficiency and photothermal stability under 808 nm NIR laser.

2. MATERIAL AND METHOD

Synthesis of GMP Nanocomposites

50.0 mg graphite oxide was added to 25 mL deionized water (DI) with a concentration of 0.1 M DBSA. The mixture was ultrasonicated for 60 min to obtain GO dispersion. Monomer solution was prepared by adding 300 µL aniline to 20 mL DI with a concentration of 0.1 M DBSA. Then monomer solution was added to GO dispersion and resultant mixture was ultrasonicated and stirred for 30 min. Afterwards, three separate $KMnO_4$ solutions were prepared according to $KMnO_4$/aniline molar ratio; 0.5, 1.0, and 1.5. $KMnO_4$ solution was then added to GO-aniline mixture to initiate simultaneous polymerization and MnO_2 formation in an ice bath. After

polymerization was completed, the samples were centrifuged with absolute ethanol and DI numerous times and dried in a vacuum oven at 65°C. Samples were named according to their $KMnO_4$/aniline ratios, namely GMP 0.5, GMP 1.0 and GMP 1.5.

Characterization

Characterization of samples were carried out by UV-Visible spectrophotometer (Shimadzu, UV-1601), X-ray diffractometer (Rigaku, Miniflex-600, Cu-K_α, $\lambda = 1.54056$ Å), and scanning electron microscope (SEM) (Quanta, 400F).

Photothermal Heating Experiments

Photothermal heating experiments were performed using an 808 nm wavelength laser (Power Technology Inc., Grande) equipped with a power-meter (Newport, 843-R). Nanocomposite dispersions were prepared at 0.06, 0.08, and 0.1 mg/mL concentrations and irradiated for 10 min at 0.8, 1.0, and 1.6 W/cm^2 power densities. Temperature values were recorded with a handheld thermal camera (FLIR, E50) and temperature versus time plots were obtained. In order to calculate the efficiency (η) time-constant method was applied (Soysal et al., 2022). Time versus $-\ln(\Delta T/\Delta T_{max})$ data were plotted during the cooling phase and the slope resulted in time-constant (τ) which is expressed by equation (1):

$$\tau = \frac{mC_p}{hA} \tag{1}$$

where, m is the mass of the dispersion, C_p is the heat capacity of the dispersion, h is the heat transfer coefficient, and A is the area perpendicular to the heat transfer. Since the dispersions were diluted, C_p value of water was used. Efficiency values were calculated using equation (2):

$$\eta = \frac{hA\Delta T_{max} - Q_{water}}{P(1 - 10^{-A})} \tag{2}$$

where, Q_{water} is the heat absorbed by water, P is the laser power, and A is the absorbance value obtained at 808 nm wavelength. Q_{water} was calculated using equation (3) by performing a heating experiment with deionized water:

$$Q_{water} = mC_{p,water}\Delta T_{max,water} \tag{3}$$

3. RESULTS AND DISCUSSION

UV-Visible spectrums of GMP 0.5, GMP 1.0, and GMP 1.5 were given in Figure 1a. GMP 0.5 shows the absorption band at 325 nm, which indicates π – π* transition of benzenoid segment of PANI (Ding, 2009). Absorption band at 400 – 450 nm corresponds to emeraldine salt phase of PANI, which can be observed in all samples (Ding, 2009). Absorption band between 700 – 1000 nm in GMP 0.5 and 500 – 750 nm in GMP 1.0 and GMP 1.5 corresponds to localized polaron bands of PANI (Ding, 2009). This blueshift and decreased absorbance in GMP 1.0 and GMP 1.5 are related to higher amount of MnO_2 in the samples. Increasing MnO_2 boosts the quantity of high oxidation state complexes in PANI and decreases degree of doping, which contributes to PANI deposition on MnO_2. This suggests how improved emeraldine structures have emerged in GMP 0.5 (Jianjun et al., 2011). It is clear that amount of $KMnO_4$ salt used both as a precursor for MnO_2 nanoparticles and as polymerization initiator, plays an important role for the fabrication of PANI structures. UV-Visible spectrums of GMP 0.5 with concentrations 0.06, 0.08, and 1.0 mg/mL and absorbance at 808 nm versus concentration plots are presented in Figure 1b and 1c. The linearity of absorbance with concentration shows the high stability of the dispersions, which is crucial for photothermal applications.

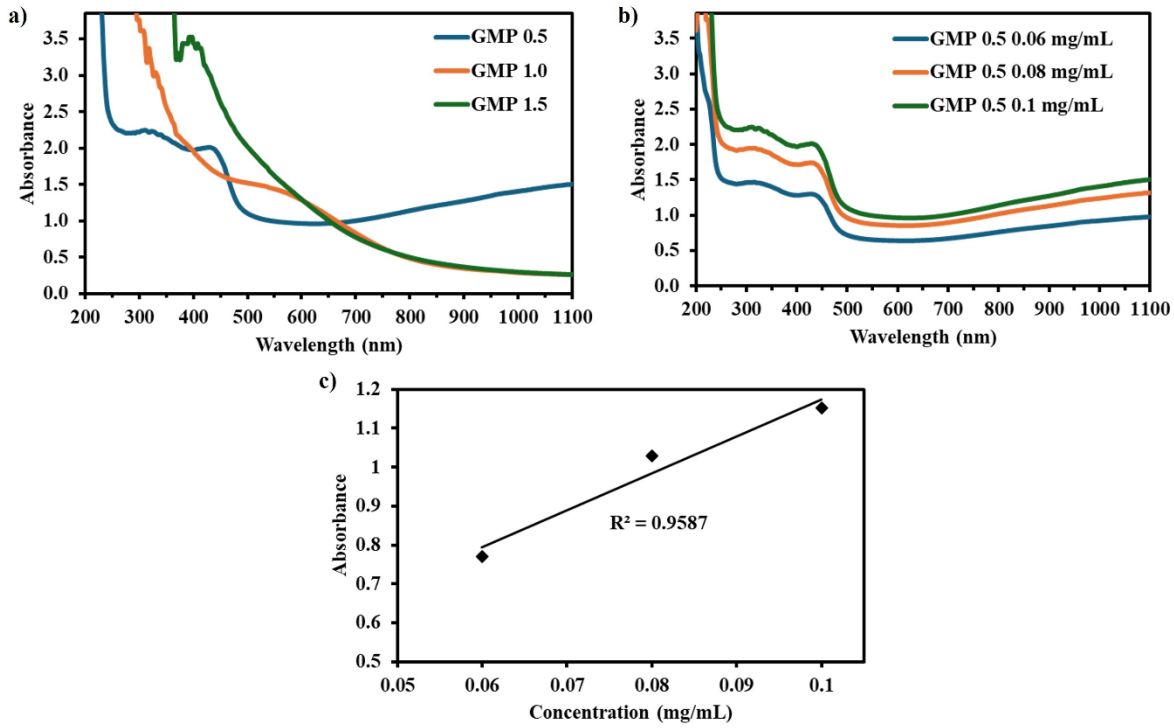

Figure 1. a) *UV-Visible spectrums of GMP 0.5, GMP 1.0, and GMP 1.5 at 0.1 mg/mL concentration,* ***b)*** *UV-visible spectrums of GMP 0.5 sample at 0.06, 0.08, and 0.1 mg/mL concentrations,* ***c)*** *Absorbance versus concentration plot of GMP 0.5*

X-ray diffraction patterns of GMP 0.5, GMP 1.0, and GMP 1.5 are given in Figure 2. All samples show the characteristic peaks of (020) and (200) planes of PANI at 19.52 and 26.02°, respectively (Çıplak & Yıldız, 2019). The prominence of PANI peaks in GMP 0.5 shows that the sample contains more polymeric structure than GMP 1.0 and GMP 1.5, in accordance with UV-visible results. At 26.20°, 37.32°, and 43.50° (310), (211), and (301) planes of α-MnO_2 (JCPDS No: 00-014-0644) can be observed (Izwan Misnon & Jose, 2021). In GMP 1.0 and GMP 1.5 samples (002) plane of GO is seen at 9.90° (Yürekli Bayar et al., 2023). The absence of this peak in GMP 0.5 might be due to complete coverage of GO with PANI structure.

Figure 3 displays SEM images of GO and GMP nanocomposites. GO nanosheets have a film structure with crooked and folded edges. It is noticed that, GMP nanocomposites exhibits different morphologic features according to their $KMnO_4$/aniline ratios. In GMP1 and GMP1.5 samples, where high amounts of $KMnO_4$ were used, MnO_2 nanostructures in the form of needles and nanoparticles can be seen on the surface of GO nanosheets within the polymer matrix. On the other hand, it was determined that in the GMP0.5 nanocomposite, where $KMnO_4$/aniline molar ratio was the highest, polymer production was higher, consistent with the UV-Visible spectrum of the samples, GO and MnO_2 nanostructures were embedded in the polymer matrix. It was also observed that the polymer matrix consisted of small-sized polymeric nanostructures. This situation is thought to be due to the strong interaction between the aniline monomer and the GO nanosheet, the fact that $KMnO_4$ is an effective oxidation agent for the monomer as well as being a source of MnO_2, and the role of DBSA as a stabilizing agent that prevents the composite from forming large agglomerations.

Firstly, to determine the nanocomposite with the highest efficiency, dispersions of GMP 0.5, GMP 1.0, and GMP 1.5 were prepared at 0.1 mg/mL concentration and irradiated at 1.0 W/cm^2 for 10 min and cooled for 20 min. Heating and cooling curves of the nanocomposites are given in Figure 4a. Highest temperature difference was obtained with GMP 0.5 as 34.7°C. Temperature difference values of GMP 1.0 and GMP 1.5 were 22.1 and 24.7°C, respectively. $-\ln(\Delta T/\Delta T_{max}) - t$ plots of nanocomposites were given in Figure 4b. Time constants of GMP 0.5, GMP 1.0, and GMP 1.5 were found as 312.47, 468.39, and 466.85, respectively. Applying equation (2) efficiency values were calculated as 73.9 % for GMP 0.5, 42.8 % for GMP 1.0, and 47.4 % for GMP 1.5. The highest temperature and efficiency values were achieved with GMP 0.5 nanocomposite, thus further experiments were performed using GMP 0.5.

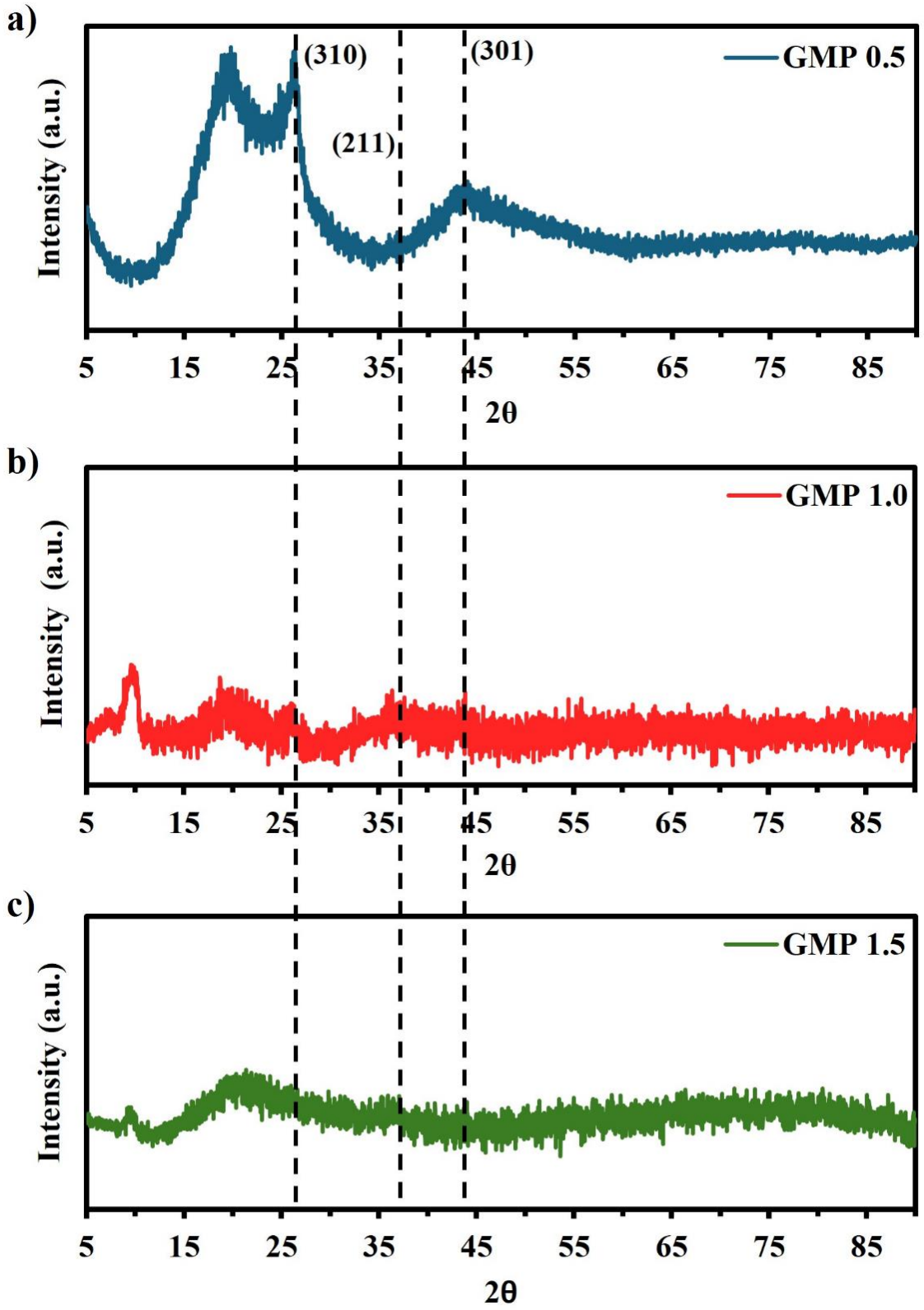

Figure 2. *X-ray diffraction patterns of* ***a)*** *GMP 0.5,* ***b)*** *GMP 1.0,* ***c)*** *GMP 1.5*

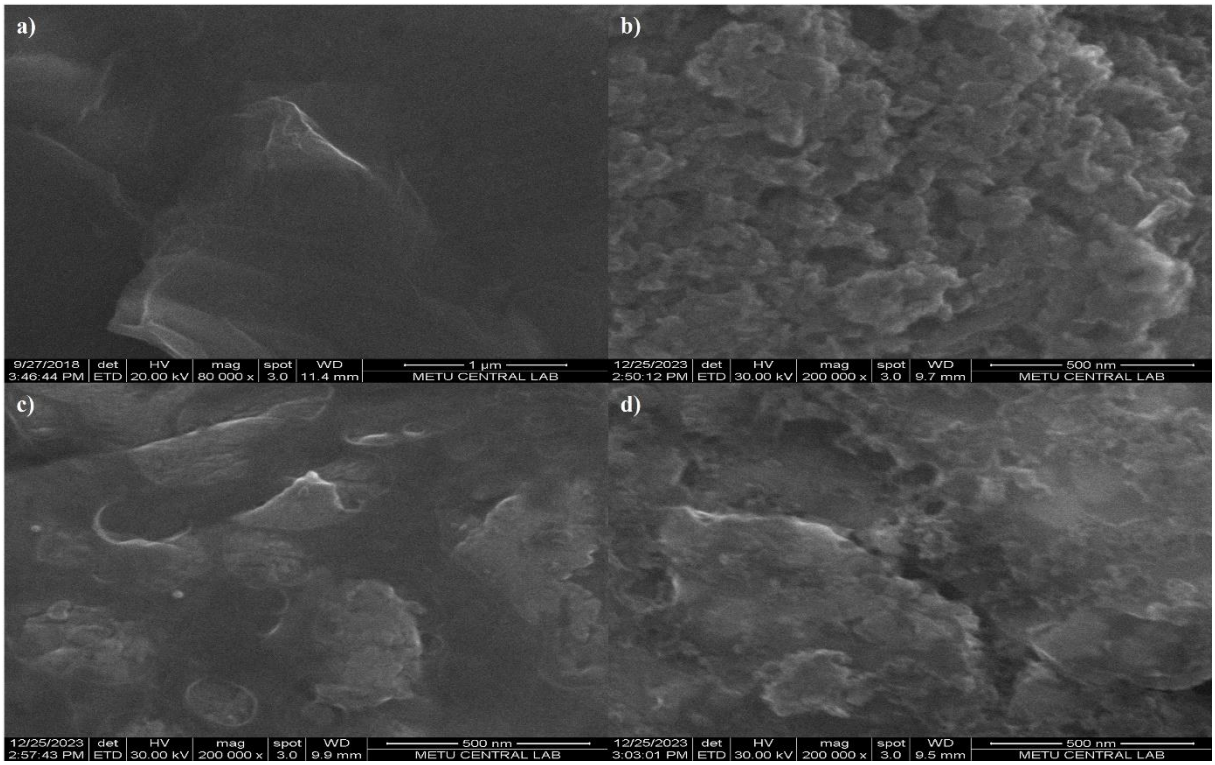

Figure 3. *SEM images of* ***a)*** *GO* ***b)*** *GMP 0.5,* ***c)*** *GMP 1.0,* ***d)*** *GMP 1.5*

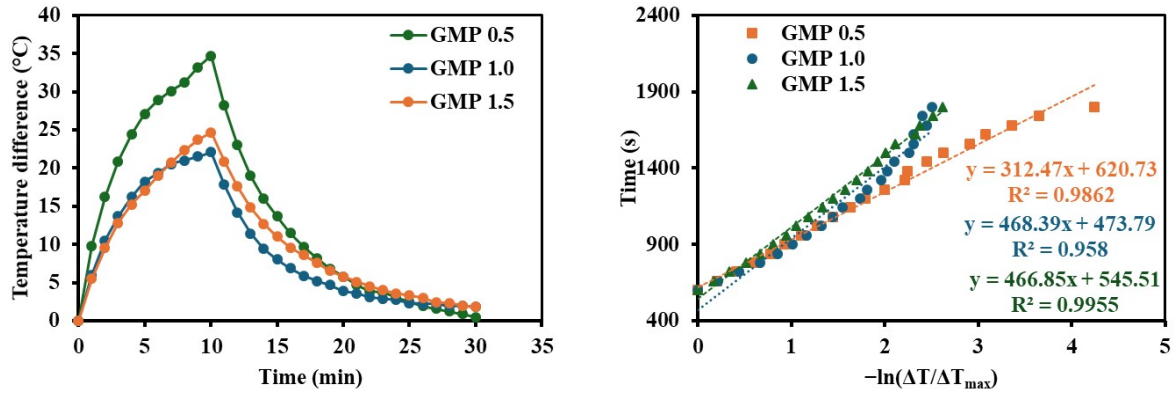

Figure 4. a) *Heating and cooling curves of GMP 0.5, GMP 1.0, and GMP 1.5,* ***b)*** *– ln(ΔT/ΔTmax) – t plots of GMP 0.5, GMP 1.0, and GMP 1.5*

In order to further evaluate the performance of GMP 0.5 sample, varied laser power densities were used to irradiate nanocomposite dispersions at varied concentrations. Heating curves of GMP 0.5 dispersions having concentrations of 0.06, 0.08, and 0.1 mg/mL and deionized water were given in Figure 5 a-c. At 0.8 W/cm^2 laser intensity, maximum temperatures of GMP 0.5 dispersions achieved were found to be 50.3, 55.6, and 54.7°C for 0.06, 0.08, and 1.0 mg/mL, respectively. Temperature difference of deionized water for this laser power density was only 1.3°C. Increasing power density to 1.0 W/cm^2 yielded in slightly increased maximum temperatures of 53.2, 57.8, and 57.9°C for 0.06, 0.08, and 1.0 mg/mL, respectively. Temperature difference of deionized water was found to be 1.6°C at 1.0 W/cm^2. Further increase in laser power density resulted in elevated maximum temperatures. At 1.6 W/cm^2, 0.06, 0.08, and 1.0 mg/mL dispersions were heated up to 70.8, 74.7, and 75.5°C. At this laser power density maximum temperature difference for deionized water was only 2.6°C. The maximum temperature differences obtained for nanocomposites were given in Figure 5d. Expectedly, the maximum temperatures of all samples increased with increasing laser intensity. At 1.6 W/cm^2 laser power density, increasing concentration resulted in increased maximum temperatures. However, at 0.8 W/cm^2, the maximum temperature of 0.08 mg/mL dispersion were higher than that of 0.1 mg/mL.

Additionally, at 1.0 W/cm^2, the maximum temperature differences of 0.08 and 0.1 mg/mL were identical. These may be due to the laser power densities being relatively low as well as concentrations being close.

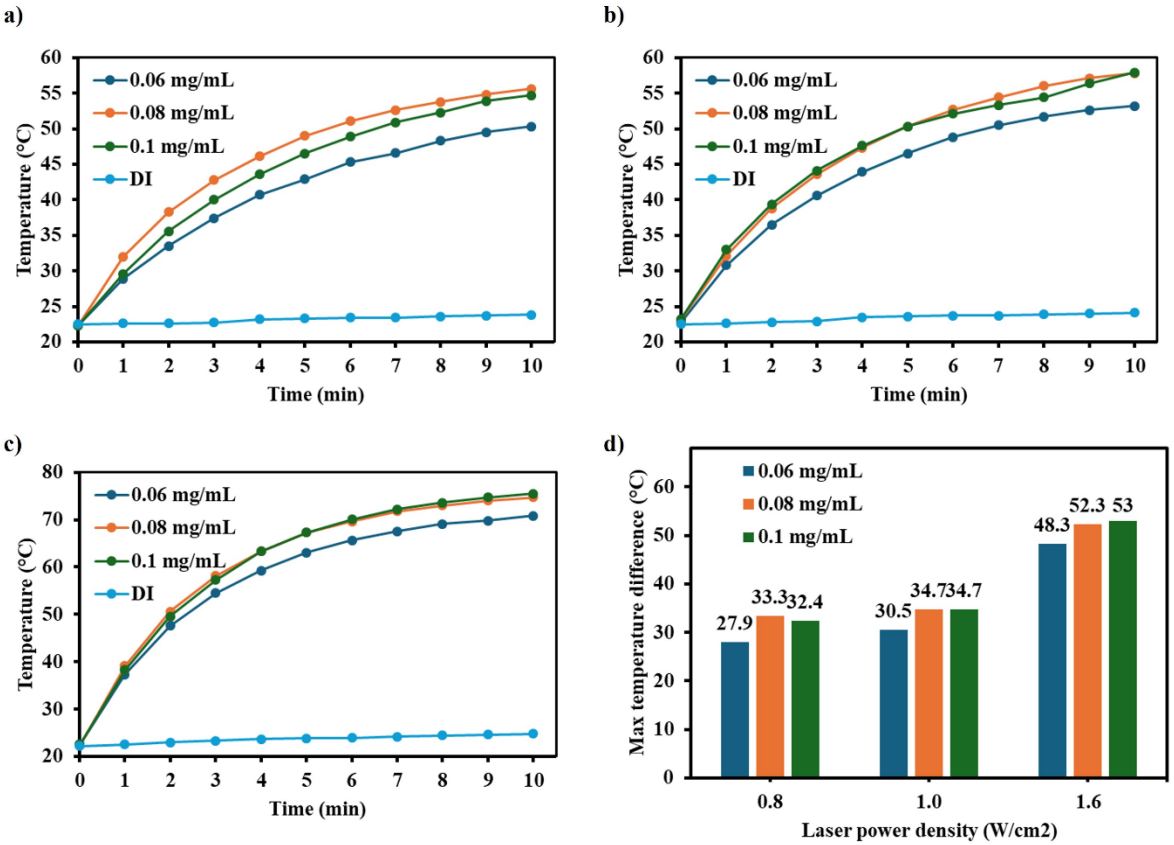

Figure 5. *Heating curves of GMP 0.5 and deionized water* ***a)*** *at 0.8 W/cm^2,* ***b)*** *at 1.0 W/cm^2,* ***c)*** *at 1.6 W/cm^2,* ***d)*** *achieved maximum temperature differences at different laser power densities*

Further evaluation of the photothermal performance of GMP 0.5 nanocomposite was performed by cyclic heating cooling experiments shown in Figure 6. A total of 6 cycles were exercised to GMP 0.5 dispersion with 0.1 mg/mL concentration at 1.0 W/cm^2 intensity. Maximum temperature values for the cycles were recorded as 57.9, 57.3, 58.7, 58.2, 57.8, and 58.7°C. There was no discernible shift in the highest temperature, which demonstrated the strong stability and high photothermal ability of the nanocomposite.

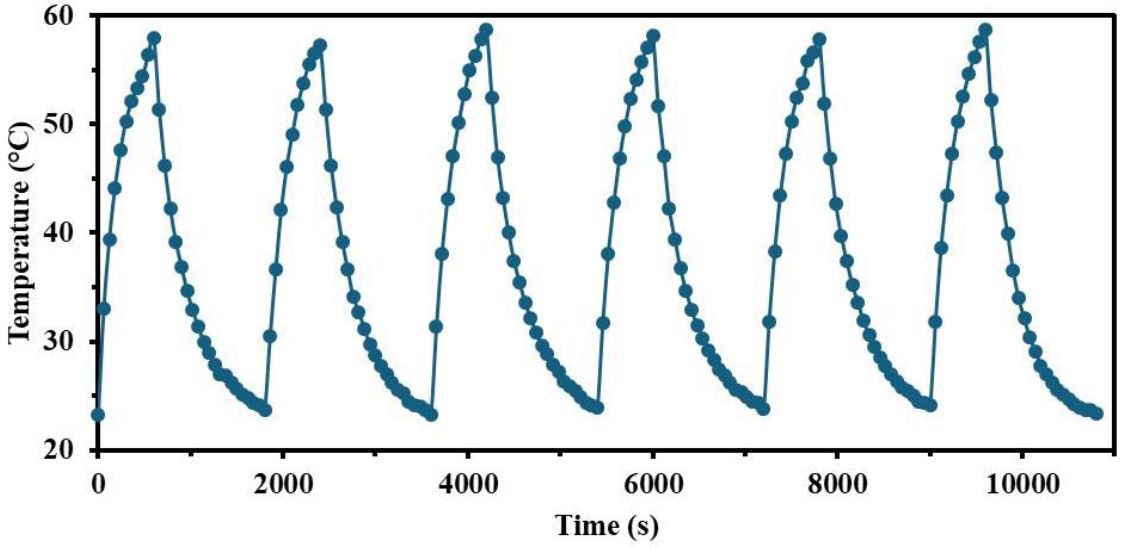

Figure 6. *Cyclic heating cooling experiments for GMP 0.5 0.1 mg/mL at 1.0 W/cm^2*

4. CONCLUSION

GO-MnO_2-PANI nanocomposites were fabricated by simultaneous aniline polymerization and MnO_2 formation over GO nanosheets. It has been seen that amount of $KMnO_4$ salt in the synthesis procedure plays an important role for PANI formation. The use of DBSA both as a stabilizing and doping agent, enabled water-stable dispersions, which is essential for photothermal exercises. The photothermal properties of the nanocomposites were tested for the first time in literature. The efficiency of GMP 0.5 nanocomposite was obtained as high as 73.9 %. Moreover, the cyclic heating cooling experiments demonstrated that the nanocomposite can be used in practical photothermal applications without a loss in its performance. These findings show that GO-MnO_2-PANI nanocomposites can be employed in both photothermal cancer treatment and antibacterial applications because of their strong NIR absorption, stable dispersion forming abilities, and high cyclic performances.

AUTHOR CONTRIBUTIONS

Conceptualization, Z.Ç. and F.S.; methodology, Z.Ç. and F.S.; title, F.S., validation, Z.Ç. and F.S.; laboratory work, Z.Ç. and F.S.; formal analysis, Z.Ç. and F.S.; research, Z.Ç. and F.S.; sources, Z.Ç. and F.S.; data curation, Z.Ç. and F.S.; manuscript-original draft, Z.Ç. and F.S.; manuscript-review and editing, Z.Ç. and F.S.; visualization, F.S.; supervision, Z.Ç.; project management, Z.Ç. and F.S.; funding, Z.Ç. and F.S.; All authors have read and legally accepted the final version of the article published in the journal.

CONFLICT OF INTEREST

The authors declare no conflict of interest.

REFERENCES

Bai, X., Yang, Y., Zheng, W., Huang, Y., Xu, F., & Bao, Z. (2023). Synergistic photothermal antibacterial therapy enabled by multifunctional nanomaterials: progress and perspectives. *Materials Chemistry Frontiers*, *7*(3), 355-380. https://doi.org/10.1039/D2QM01141G

Çıplak, Z., & Yıldız, N. (2019). Polyaniline-Au nanocomposite as electrode material for supercapacitor applications. *Synthetic Metals*, *256*, 116150. https://doi.org/10.1016/j.synthmet.2019.116150

Ding, K.-Q. (2009). Cyclic Voltammetrically Prepared MnO2 -Polyaniline Composite and Its Electrocatalysis for Oxygen Reduction Reaction (ORR). *Journal of the Chinese Chemical Society*, *56*(5), 891-897. https://doi.org/10.1002/jccs.200900132

Guan, G., Win, K. Y., Yao, X., Yang, W., & Han, M. (2021). Plasmonically Modulated Gold Nanostructures for Photothermal Ablation of Bacteria. *Advanced Healthcare Materials*, *10*(3). https://doi.org/10.1002/adhm.202001158

İrez, A. B., & Bayraktar, E. (2020). Design of Epoxy Modified Recycled Rubber-Based Composites: Effects of Different Contents of Nano-Silica, Alumina and Graphene Nanoplatelets Modification on the Toughening Behavior. *Gazi University Journal of Science*, *33*(1), 188-199. https://doi.org/10.35378/gujs.585446

Izwan Misnon, I., & Jose, R. (2021). Charge storage in the PANI–α-MnO_2 polymer–nanocomposite system. *Materials Today: Proceedings*, *41*(3), 513-519. https://doi.org/10.1016/j.matpr.2020.05.235

Jianjun, H., Yuping, D., Jia, Z., Hui, J., Shunhua, L., & Weiping, L. (2011). γ-MnO_2/polyaniline composites: Preparation, characterization, and applications in microwave absorption. *Physica B: Condensed Matter*, *406*(10), 1950-1955. https://doi.org/10.1016/j.physb.2011.02.063

Lima-Sousa, R., Melo, B. L., Mendonça, A. G., Correia, I. J., & de Melo-Diogo, D. (2024). Hyaluronic acid-functionalized graphene-based nanohybrids for targeted breast cancer chemo-photothermal therapy. *International Journal of Pharmaceutics*, *651*, 123763. https://doi.org/10.1016/j.ijpharm.2023.123763

Liu, J., Feng, L., & Wu, Y. (2021). Enzymatically synthesised MnO_2 nanoparticles for efficient near-infrared photothermal therapy and dual-responsive magnetic resonance imaging. *Nanoscale*, *13*(25), 11093-11103. https://doi.org/10.1039/D1NR02400K

Pham, T.-T. D., Phan, L. M. T., Nam, S.-N., Hoang, T. X., Nam, J., Cho, S., & Park, J. (2024). Selective photothermal and photodynamic capabilities of conjugated polymer nanoparticles. *Polymer*, *294*, 126689. https://doi.org/10.1016/j.polymer.2024.126689

Soysal, F., Çıplak, Z., Getiren, B., Gökalp, C., & Yıldız, N. (2022). Fabrication of polypyrrole enveloped reduced graphene oxide/iron oxide and determination of its photothermal properties. *Materials Research Bulletin*, *150*, 111792. https://doi.org/10.1016/j.materresbull.2022.111792

Wang, X., Su, K., Tan, L., Liu, X., Cui, Z., Jing, D., Yang, X., Liang, Y., Li, Z., Zhu, S., Yeung, K. W. K., Zheng, D., & Wu, S. (2019). Rapid and Highly Effective Noninvasive Disinfection by Hybrid Ag/CS@MnO 2 Nanosheets Using Near-Infrared Light. *ACS Applied Materials & Interfaces*, *11*(16), 15014-15027. https://doi.org/10.1021/acsami.8b22136

Wei, W., Zhang, X., Zhang, S., Wei, G., & Su, Z. (2019). Biomedical and bioactive engineered nanomaterials for targeted tumor photothermal therapy: A review. *Materials Science and Engineering: C*, *104*, 109891. https://doi.org/10.1016/j.msec.2019.109891

Xing, Z., Dong, B., Zhang, X., Qiu, L., Jiang, P., Xuan, Y., Ni, X., Xu, H., & Wang, J. (2024). Cypate-loaded hollow mesoporous Prussian blue nanoparticle/hydrogel system for efficient photodynamic therapy/photothermal therapy dual-modal antibacterial therapy. *Journal of Biomedical Materials Research Part A*, *112*(1), 53-64. https://doi.org/10.1002/jbm.a.37613

Xu, W., Qing, X., Liu, S., Chen, Z., & Zhang, Y. (2022). Manganese oxide nanomaterials for bacterial infection detection and therapy. *Journal of Materials Chemistry B*, *10*(9), 1343-1358. https://doi.org/10.1039/D1TB02646A

Yu, C., Xu, L., Zhang, Y., Timashev, P. S., Huang, Y., & Liang, X.-J. (2020). Polymer-Based Nanomaterials for Noninvasive Cancer Photothermal Therapy. *ACS Applied Polymer Materials*, *2*(10), 4289-4305. https://doi.org/10.1021/acsapm.0c00704

Yürekli Bayar, E., Getiren, B., Soysal, F., Çıplak, Z., Yıldız, N., & Bayraktar, E. (2023). Graphene oxide/polyaniline/silver nanocomposite synthesis and photothermal performance. *Materials Research Bulletin*, *166*, 112352. https://doi.org/10.1016/j.materresbull.2023.112352

Zeplin, G., & Neiva, E. G. C. (2021). One-pot green synthesis of graphene oxide/MnO2/polyaniline nanocomposites applied in aqueous and neutral supercapacitors and sensors. *Journal of Electroanalytical Chemistry*, *902*, 115776. https://doi.org/10.1016/j.jelechem.2021.115776